JOURNAL OF NANO- AND ELECTRONIC PHYSICS
Vol. **17** No 2, 02022(5pp) (2025)

ЖУРНАЛ НАНО- ТА ЕЛЕКТРОННОЇ ФІЗИКИ
Том **17** № 2, 02022(5cc) (2025)

OPEN ACCESS

REGULAR ARTICLE

6.6 GHz Single Element 2 × 4 Massive MIMO Antenna in 6G Devices

D. Kumutha[1,*] ✉, P. Geetha[2], P. Gobi[3], K. Tamilarasi[4], S. Rajesh[1], S. Sivakami[5]

[1] *Department of CSE, Jeppiaar Institute of Technology, Kunnam, Sripermudur, 631604 Chennai, India*
[2] *Department of Electronics and Communication Engineering, Karpaga Vinayaga College of Engineering and Technology, 603308 Chennai, India*
[3] *Department of ECE, Jeppiaar Institute of Technology, Kunnam, Sripermudur, 631604 Chennai, India*
[4] *Department of IT, Panimalar Engineering College, Chennai, India*
[5] *Department of ECE, New Prince Shri bhavani college of engineering and Technology, Chennai, India*

(Received 10 February 2025; revised manuscript received 15 April 2025; published online 28 April 2025)

These days, 6G and massive MIMO (multiple input multiple output) technologies greatly enhance wireless communication. Conventional approaches are proven to be ineffective in 5G specifications and to have increased interference in MIMO antennas. The two truncated linear patches have a ground performance of 37.6 mm × 33.4 mm in the substrate and an antenna size of 9.2 m, 7.1 mm at the top layer. It is suggested that the 2 × 4 MIMO antenna's dimensions for 75 mm, 33 mm, and 1.6 mm be improved by the 6G specification. With a centre frequency of 6.6 GHz, the planned Massive MIMO with 6G is regulated to function between the 4 to 5.7 GHz range. This article displays a maximum gain of 24.4 dBi and a 3.9 dB gain fluctuation at 6.6 GHz. By using HFSS simulated results for operating frequency, the suggested system can improve performance by offering isolation of 16 dB, directivity of 4.9, and relative permittivity of 4.4. Furthermore, inserting the 2 × 4 single-element Massive MIMO Antenna, which can perform spatial multiplexing for the 6G application, has resulted in a gain of 11.16 dBi with an 86 % radiation efficiency. This design supports for the 6G devices which is used for the wireless communication.

Keywords: 6G, Massive MIMO, HFSS, Linear patch, Mobile Communication, Efficiency.

DOI: 10.21272/jnep.17(2).02022 PACS number: 84.40.Ba

1. INTRODUCTION

A multi-frequency MIMO antenna designed for 5G as well as Wi-Fi 6E applications is presented in this research. To create tri-band electromagnetic radiation, this antenna uses a split-ring the resonators (SRR) construction along with a cosine-shaped monopole. SRR, folding split-ring resonators (FSRR), with Archimedean helical metasurfaces that have splitting are used to provide a frequency range extension through the integration of spatial wave and electromagnetic surface wave uncoupling techniques. Space wave decoupling over the tri-band is made possible by the Archimedean helical metasurface. A small antenna is produced by combining wave propagation with air space wave separation methods. The modeled data and the observed findings agree quite well. In particular, the observed findings demonstrate isolation gains of 3.6 dB, 37.58 dB, and 7.32 dB covering the frequency ranges 3.45–3.55 GHz, 5.7–5.9 GHz, and 6.75–7 GHz, correspondingly, along with a corresponding reflection coefficient of – 10 dB. Additionally, the MIMO antenna has a spatial correlation index (SCI) of 0.0025 and typical average efficacy of about 89 %. Furthermore, immediately following the metasurface is incorporated, the antenna's maximum gain rises by 4.3 dB at 3.5 GHz, 3.8 dB at 5.8 GHz, and 1.9 dB at 6.9 GHz. It is anticipated that this design and technique will greatly improve separating in multi-frequency MIMO antennas.

The technique of the industrialization of 5G systems has now started in the electronic communications industry due to the advancement of contemporary wireless communication technologies. The deep incorporation of innovative infrastructures like the Internet of Things, AI, as well as Industrial Internet of Things combined with actual economic activity is being accelerated by the 5G communication system, which is a versatile, multiple levels, and technology-converged network [1, 2]. It is commonly known that multipath features can be used by wide-bandwidth along with MIMO technologies to increase spectrum effectiveness and channel capacity without raising input power, which in turn improves wireless systems for the maximum throughput [3-5].

Even though mobile gadgets now use 2 × 2 [6, 7] and 4 × 4 MIMO [8-10] antenna systems, that operate far slower than the 10 Gpbs peak information rate, these are still unable to meet 5G communication standards. Thus, adding extra antennas to cellphones has grown into a trend that cannot be avoided. Scholars are paying more and more attention to developing antenna arrays that are both high-performing and economical. In earlier research, MIMO systems with eight, ten, twelve, and sixteen antenna arrays were developed for smartphones operating in LTE bands [11-18]. In order to obtain

* Correspondence e-mail: skvijaykumu@gmail.com

Cite this article as: D. Kumutha et al., *J. Nano- Electron. Phys.* 17 No 2, 02022 (2025) https://doi.org/10.21272/jnep.17(2).02022

higher isolation, a basic antenna array structure design just incorporates a reversed U-shaped emitting element and vertical stubs imprinted on the bilateral substrates; zero decoupling architecture is introduced [15].

However, the segregation among the antenna components drastically reduces as the total number of antenna components in an mobile device system rises. Upcoming antenna layouts should prioritize the methodologies of decoupling as well as antenna shrinking in order to solve this issue. To increase isolation and lower ECC values, researchers used extra decoupling strategies or particular antenna configurations and structures in the majority of antenna design studies. A defective grounded structure, an orthogonal phase method [16], and a decoupling network are the three primary decoupling strategies amongst them.

The Internet of Things (IoT) is a significant application of wireless sensor networks (WSNs) in 5G systems, necessitating large-scale wireless data transmission. As a result, massive multiple-input multiple-output (M-MIMO) is now recognized to be an important technique and paradigm for mobile phone networks that go exceed fifth-generation (B5G) in the near future. But having more antennas additionally renders the receiving end more complicated, which presents a problem which requires to be solved. In order the upstream portion of M-MIMO orthogonal frequency division multiplexing (OFDM) along with universal filtered multi-carrier (UFMC) systems, we suggest a unique multi-user detection (MUD) system to minimize the bit error rate (BER), restrict the amount of computation needed, and design a technique for detection appropriate across both 4G as well as B5G circumstances. This technique, known as mixed over-relaxation (MOR), incorporates the advantages of accelerated over-relaxation (AOR) along with successive over-relaxation (SOR).

The MOR process is divided into two stages: the initial stage, which generates suitable for collaboration stage, that guarantees lightning-fast convergence as well as enhanced efficiency via exchanging repetitions, along with the initial criteria to improve scalability and reduce divergence hazard. Modeling analysis demonstrate that our suggested identification technique achieves 99.999 % and 99.998 % enhancements in BER efficiency, accordingly, when contrasted with conventional SOR and AOR approaches. In contrast to prior repetitive techniques, this study presents an innovative collaborative receiver design that improves BER performance and increases the convergence rate by utilizing the speeding up the characteristics of the AOR algorithm combined with the elongation qualities of the SOR algorithm.

Crucially, the combination of the convergent process strengths as well as complementary aspects of AOR along with the SOR enables such superior BER efficacy. Quantitative results confirm that, contrast to other detection methods under similar conditions, our approach achieves better BER performance and approximates the performance of the minimum mean square error (MMSE) method. While our method adds slightly more The computational demands in contrast to detectors that use CSOR and CAOR with the same number of iterations, the MOR detector requires fewer iterations to converge, and its BER performance closely matches that of MMSE. Thus, our proposed method balances excellent BER performance with moderate complexity, outperforming additional detectors that need to be iterated. Moreover, implementing MOR in B5G as well as 4G contexts shows that it is well-suited for these scenarios, fully demonstrating its potential. Finally, the B5G system is a key enabler for sophisticated networks of wireless sensors, as well as AIoT applications encounter significant computational and difficulties with transmission. It is therefore Unavoidable that technologies meeting the demands of eMBB, URLLC, and mMTC will continue to evolve. The MOR algorithm, with its lower complexity and superior BER performance, is well-positioned to address the need for great precision, minimal latency, with enormous scale distribution in this area, making it a promising candidate for future development.

The present work is structured in the following manner: The detailed introduction and its literature survey is explained in detail in section 1. The analysis of the MIMO antenna's design concepts, procedure, and decoupling mechanism is covered in detail in Section 2. Antenna performance, including ECC, effectiveness, as well as gain structures, is analyzed in Section 3 by contrasting antennas either with or without mechanisms for separation. The design procedure, techniques, and outcomes of the MIMO antenna created in this paper are compiled in Section 4.

2. DESIGN OF MIMO WIDEBAND ANTENNA SYSTEMS

2.1 Design and Evaluation of Antenna Elements

The prevalent wireless transmission device for sending electromagnetic radiation via space is known as a microstrip patch antenna. The substrate, patch, ground as well as feed are the four main components of a microstrip patch antenna.

Amongst various shapes, it comes in square, elliptical, circular, rectangular, and ring forms. It is made up of a ground plane on one side and a dielectric constant on the other. Applications for microstrip patch antennas include global positioning systems (GPS), automobile, logistics tracking, and microwave communication. A microstrip antenna is depicted in Figure 1 with W representing width, L representing length, and ε_{reff} representing the rectangular patch's effective dielectric constant [3].

Since it is commonly recognized that patch antennas must be installed on printed circuit boards (PCBs) for a variety of communication devices, this portion addresses developing and layout of a wireless transmission patch antenna. For applications in wireless networks, researchers created a variety of antenna patch layouts in response to feature. IE3D, HFSS, CST, MATLAB, and additional computational tools can be used to build, model, and evaluate microstrip antennas. Figure 2 shows the antenna's evaluations, which include the ground, patch, substrate, and feed line lengths and widths. The micro strip patch antenna was designed, developed, and modeled in the CST microwave studio.

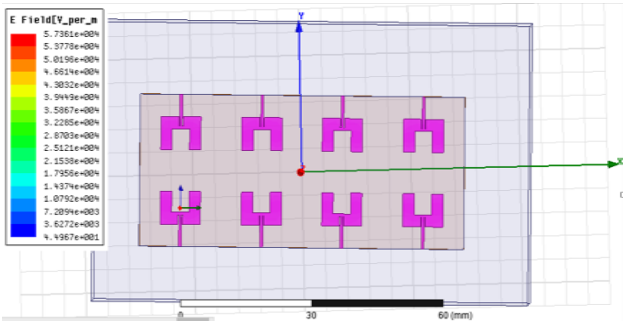

Fig. 1 – The designed wideband antenna array

A *T*-shaped 50-ohm microstrip line is used to supply power in all three of the antenna component's design scenarios depicted in Figure 1 in regards to adequately assess the design procedure of the suggested antenna element. A *C*-shaped radiating component is present on the substrate's vertical side in Case 1. The resonant antenna's frequency component is 3.6 GHz, according to the *S*-parameter leads to from the CST simulation, as depicted in Figure 2. However, as illustrated in Figure, current is concentrated on the *T*-shaped intake line while the electrical current on the a *C*-type emitted component is almost nil due to the substantial reflecting coefficient and inadequate matching impedance. Nevertheless, by incorporating a rectangular radiated component is situated on the left side end of the *T*-shaped like a microstrip line that includes a *U*-shaped slot on most of the ground plane of the substrate itself, Case 2 is formed from Case 1.

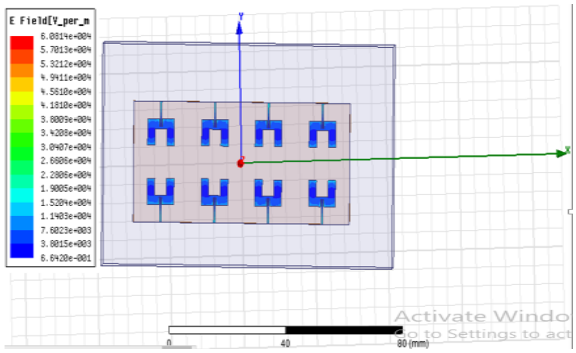

Fig. 2 – Detailed description of the antenna element's framework

In Case 2, as illustrated in Figure 2, while current resides between the *U* shaped like a slot as well as the left rectilinear emitting component, the *T*-shaped feeding line transmits electromagnetic radiation upwards to the *C*-shaped emitting element. The *C*-shaped emitting component's electrical current is reduced to zero, although it is still low on its two side arms. In order to solve these issues, Bending methods according to Case 2 were used to transform the *C* like shaped radiated component into a radiating component that loops and meanders.

The evaluation of the *S*-parameters in Figure 2 shows that the resonance frequency moves to the left, forming an additional resonance point, increasing the functional bandwidth to 400 MHz, leading to broadband performance and better impedance compatibility. Comparing the radiating components to those in Case 2, Figure 2 demonstrates that the current is primarily spread along the edges of the *U*-shaped slot along with the meandering, looping radiating component, greatly enhancing their efficiency.

3. RESULTS AND ITS DISCUSSION

3.1 *S*-Parameters Analysis

Figure 3 displays the modeling and measurement of the *S*-parameters for the 12-element wideband antenna system. A broader – 6 dB bandwidth (3.2–3.7 GHz) as well as excellent matched impedance throughout the necessary frequency band for reflecting coefficients are made possible by the directional antenna array's identical framework (S11 = S66, S22 = S55, and S33 = S44), as shown in Figure 3. With regard to the propagation coefficients, separation among any two antennas from Ant1 to Ant12 continues to be above 12 dB (only the S21, S31, S32, S43, S71, S81, and S91s curves are visible due to the asymmetrical framework).

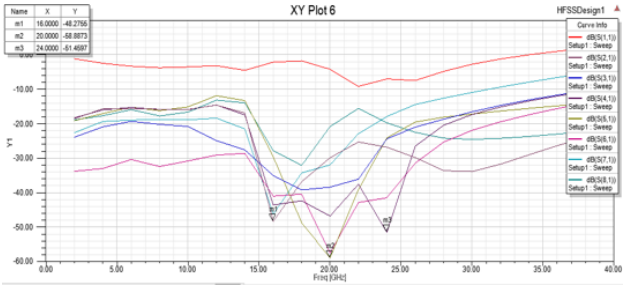

Fig. 3 – Simulation results for *S*-parameters and measurement

Additionally, as seen in Figure 3a, when Ant1 is activated, the majority of the current is focused on its meandering, looping radiating element, with very little current flowing to Ant2. This shows that Ant1 and Ant2 are well isolated from one another and that Ant1's electromagnetic radiation has minimal coupling effects on Ant2. Similarly, Figure 3b and Figure 3c display the current distributions of Ant2 and Ant3 when they are activated, respectively. The antenna elements' high degree of isolation from one another is further confirmed by the low current in the nearby antenna elements. The antenna array's layout technique, which precisely adjusts the spacing between antenna elements to lessen the metallic coupling effect, is responsible for this exceptional isolation.

3.2 Radiation Performance of Antenna Array

As illustrated by the two-dimensional far-field electromagnetic radiation configurations of Ant1 to Ant6 within the *E*-plane (phi = 0) as well as *H*-plane (phi = 90) at 3.36 GHz and 3.63 GHz frequencies, Figure 11 shows that the antenna exhibits almost omnidirectional radiation attributes in the *XOZ* plane across both frequencies, via slightly more powerful radiation in the *Z* direction. On the other hand, the antenna's distinct features are visible in the *YOZ* plane, where the + *Y* direction exhibits somewhat stronger radiation. Additionally, Figure 5 provides a 3D far-field radiation pattern that clarifies Figure 6 and enables a visual evaluation of the built antenna's radiation effectiveness.

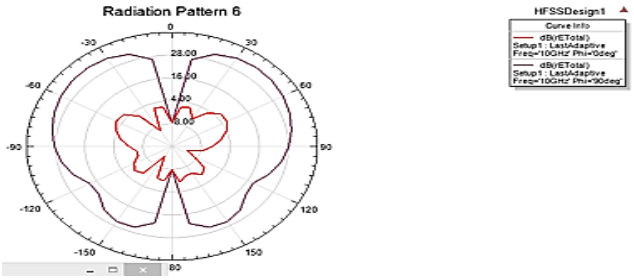

Fig. 4 – Detailed view of the Radiation Pattern for 2D far-field pattern

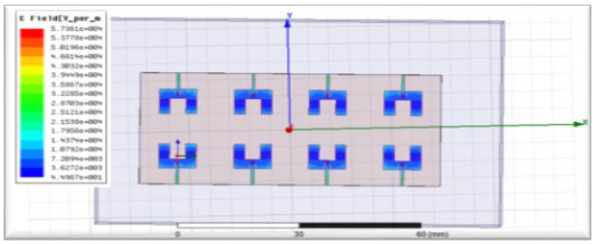

Fig. 5 – Detailed view of the U-shaped slot

Fig. 6 – Designed antenna array's 3D far-field emission patterns

Figures 5 and 6 demonstrate the mirrored symmetrical far-field propagation structures from Ant1 to Ant3 and Ant4 to Ant6 in the XOZ plane, which is in accordance with the antenna array's structure. Because of the planned MIMO antenna system's symmetrical layout, the far-field emission patterns generated by the remaining antenna components are omitted for the sake of conciseness.

All things considered, these findings show that the wideband antenna array satisfies the radiation performance requirements for smartphone antennas by possessing high gain properties within its operating frequency spectrum and omnidirectional emission.

4. CONCLUSION

The 6.6 GHz Single Element 2 × 4 Massive MIMO Antenna's design and analysis show notable progress in overcoming the drawbacks of traditional methods for wireless communication in 5G and beyond. With its improved isolation, directivity, and gain performance, the suggested antenna arrangement successfully satisfies the 6G requirements. The antenna's 75 mm × 33 mm × 1.6 mm optimized dimensions and 6.6 GHz center frequency allow it to function effectively in the 4 GHz to 5.7 GHz frequency range, guaranteeing reliable performance in high-frequency applications.

The system's capacity to provide high-speed data transmission with little interference is demonstrated by its maximum gain of 24.4 dBi and radiation efficiency of 86 %. Additionally, this antenna is appropriate for high-capacity and high-reliability applications in 6G networks due to its 16 dB isolation and spatial multiplexing capability. The effectiveness of the suggested design in reaching reliable performance parameters, like relative permittivity of 4.4 and gain fluctuation of 3.9 dB, is confirmed by the HFSS simulated results.

REFERENCES

1. S. Kumar, A.S. Dixit, R.R. Malekar, H.D. Raut, L.K. Shevada, *IEEE Access* **6**, 163568 (2020).
2. H. Li, X. Chen, X. Zhou, *ZTE Technol. J.* **21**, 14 (2015).
3. A.A. Al-Hadi, J. Ilvonen, R. Valkonen, V. Viikari, *Microw. Opt. Technol. Lett.* **56**, 1323 (2014).
4. K.L. Wong, T.W. Kang, M.F. Tu, *Microw. Opt. Technol. Lett.* **53**, 1569 (2011).
5. M. Jensen, J. Wallace, *IEEE Trans. Antennas Propag.* **52**, 2810 (2004).
6. J. Prakash, R. Vijay, S. Natarajamani, *Proceedings of the IEEE International Conference on Advances in Computing, Communications and Informatics (ICACCI)* (Udupi, India: 13–16 September 2017).
7. Y.-L. Ban, Z.-X. Chen, Z. Chen, K. Kang, J.L.-W. Li, *IEEE Antennas Wirel. Propag. Lett.* **13**, 999 (2014).
8. Y. Ding, Z. Du, K. Gong, Z. Feng, *IEEE Antennas Wirel. Propag. Lett.* **6**, 655 (2007).
9. K.L. Wong, Y.C. Chen, W.Y. Li, *Microw. Opt. Technol. Lett.* **58**, 2046 (2016).
10. H. Huang, X. Li, Y. Liu, *IEEE Antennas Wireless Propag. Lett.* **17**, 1052 (2018).
11. M.Y. Li, Y.L. Ban, Z.Q. Xu, J. Guo, Z.F. Yu, *IEEE Access* **6**, 6160 (2017).
12. K.L. Wong, J.Y. Lu, *Microw. Opt. Technol. Lett.* **57**, 1699 (2015).
13. D. Kumutha, T. Islam, V. Samudrala, S. Das, S. Asha, M. El Ghzaoui, *J. Nano- Electron. Phys.* **15** No 6, 06029 (2023).
14. M. Jeyabharathi, D. Kumutha, S. Jeevitha, P. Geetha, Manjunathan Alagarsamy, R. Delshi Howsalya Devi, *J. Nano- Electron. Phys.* **16** No 4, 04006 (2024).
15. D. Kumutha, R.D.H. Devi, C. Priya, M. Jeyabharathi, Manjunathan Alagarsamy, *J. Nano- Electron. Phys.* **16** No 3, 03007 (2024).
16. D. Kumutha, R.D.H. Devi, M. Jeyabharathi, C. Priya, Raja Manikandan, P. Geetha, *J. Nano- Electron. Phys.* **16** No 4, 04003 (2024).
17. M. Jeyabharathi, D. Kumutha, P. Geetha, R. Delshi Howsalya Devi, Raja Manikandan, T. Sripriya, *J. Nano- Electron. Phys.* **16** No 3, 03008 (2024).
18. D. Kumutha, T. Islam, P. Muthumari, K. Vijayalakshmi, R. Rajalakshmi, M. Indumathi et al., *J. Nano- Electron. Phys.* **16** No 3, 03010 (2024).
19. S. Usha, P. Geetha, A. Manimaran, S. Parasuraman, T. Karthika, Selciya Selvan, D. Kumutha, *J. Nano- Electron. Phys.* **15** No 3, 03008 (2023).

Одноелементна 6,6 ГГц 2 × 4 масивна антена MIMO в пристроях 6G

D. Kumutha[1], P. Geetha[2], P. Gobi[3], K. Tamilarasi[4], S. Rajesh[1], S. Sivakami[5]

[1] *Department of CSE, Jeppiaar Institute of Technology, Kunnam, Sripermudur, 631604 Chennai, India*
[2] *Department of Electronics and Communication Engineering, Karpaga Vinayaga College of Engineering and Technology, 603308 Chennai, India*
[3] *Department of ECE, Jeppiaar Institute of Technology, Kunnam, Sripermudur, 631604 Chennai, India*
[4] *Department of IT, Panimalar Engineering College, Chennai, India*
[5] *Department of ECE, New Prince Shri Bhavani College of Engineering and Technology, Chennai, India*

Сьогодні технології 6G та масивного MIMO (множинний вхід-множинний вихід) значно покращують бездротовий зв'язок. Традиційні підходи виявилися неефективними у специфікаціях 5G та збільшують перешкоди в антенах MIMO. Дві усічені лінійні ділянки мають наземні характеристики 37,6 мм × 33,4 мм у підкладці та розмір антени 9,2 м, 7,1 мм у верхньому шарі. Пропонується покращити розміри антени 2 × 4 MIMO для 75 мм, 33 мм та 1,6 мм за допомогою специфікації 6G. З центральною частотою 6,6 ГГц, запланований масивний MIMO з 6G регулюється для роботи в діапазоні від 4 до 5,7 ГГц. У цій статті показано максимальне посилення 24,4 дБі та коливання посилення 3,9 дБ на частоті 6,6 ГГц. Використовуючи результати моделювання HFSS для робочої частоти, запропонована система може покращити продуктивність, пропонуючи ізоляцію 16 дБ, спрямованість 4,9 та відносну діелектричну проникність 4,4. Крім того, вставка одноелементної масивної MIMO-антени 2 × 4, яка може виконувати просторове мультиплексування для застосування 6G, призвела до посилення 11,16 дБі з ефективністю випромінювання 86%. Ця конструкція підтримує пристрої 6G, які використовуються для бездротового зв'язку.

Ключові слова: 6G, Масивний MIMO, HFSS, Лінійний патч, Мобільний зв'язок, Ефективність.